Eur. Phys. J. A **8**, 361–371 (2000)

THE EUROPEAN PHYSICAL JOURNAL A

Fusion cross-section of the ^{7}Li + ^{11}B reaction

R. Vlastou[1,a], C.T. Papadopoulos[1], C. Tsabaris[1], P.A. Assimakopoulos[2], A.A. Pakou[2], G. Doukellis[3], C.A. Kalfas[3], and A.C. Xenoulis[3]

[1] National Technical University of Athens, Athens 157 80, Greece
[2] The University of Ioannina, Department of Physics, Ioannina 453 10, Greece
[3] National Research Centre "Demokritos" 153 10, Greece

Received: 10 December 1999 / Revised version: 7 May 2000
Communicated by B. Herskind

Abstract. The ^{7}Li + ^{11}B reaction has been investigated in the energy range 5.5 MeV < $E_{\rm lab}$ < 19 MeV, by detecting γ-ray resulting from the de-excitation of evaporation residues. Statistical compound-nucleus calculations have been performed in order to extract both the cross-sections of individual exit channels and the fusion cross-section of the system. The total angular momentum that the compound nucleus ^{18}O can support has been deduced and is seen to exhibit saturation for a limiting value of 8.5$\hbar$ at the high-energy extreme. The results are discussed in terms of the entrance channel and statistical yrast line limitations.

PACS. 25.70.Gh Compound nucleus – 25.70.Jj Fusion and fusion-fission reactions

1 Introduction

Considerable experimental and theoretical effort has been devoted in recent years to the understanding of the mechanism of light heavy-ion fusion reactions. Interesting systematic features have been observed and a large number of studies have been undertaken for their interpretation through macroscopic models. Most of the approaches have been essentially concentrated on the interpretation of the fusion cross-section limitations based on entrance channel or compound nucleus properties [1–6].

In the case of nuclear reactions where one of the participating ions is a light, weakly bound nucleus, such as ^{6}Li (S_α = 1.47 MeV), ^{7}Li (S_α = 2.45 MeV) and ^{9}Be ($S_{\rm n}$ = 1.67 MeV), a further tendency for the limitation of the fusion cross-section, compared to the reaction cross-section, has been observed in some systems. Omar *et al.* [7] have measured a remarkably low fusion cross-section for the ^{9}Be + ^{9}Be system, compared to heavier systems like ^{9}Be + ^{28}Si and ^{9}Be + ^{40}Ca. This behaviour has been attributed to the high probability for breaking up of ^{9}Be before the critical distance of fusion is reached.

Fusion cross-sections of ^{6,7}Li-induced reactions have also been measured at different laboratories through the γ-ray or the residual evaporation particle techniques yielding contrasting results. Thus, measurement of the fusion cross-section of ^{7}Li + ^{16}O by Scholz *et al.* [8] and ^{6,7}Li + ^{12,13}C by Mukherjee *et al.* [9,10], with the γ-ray technique, at bombarding energies up to about 10 MeV, has shown no inhibition of the fusion cross-section throughout the energy range covered. In contrast, Mateja *et al.* [11] and Dennis *et al.* [12], in a study on the evaporation residues of the same reactions at energies up to about 35 MeV, report that the fusion cross-section is about 1.5 to 2 times smaller than the total reaction cross-section even at low energies (9–12 MeV). Recently, Takahasi *et al.* [13] have observed that the fusion cross-section of the reactions ^{6,7}Li + ^{9}Be and ^{6,7}Li + ^{12}C, at energies ranging from 6 < $E_{\rm lab}$ < 33 MeV, is significantly lower than the total reaction cross-section and even smaller than the fusion cross-section expected from available systematics [3]. Similar systems, like the ^{10,11}B + ^{10,11}B reactions, have also been studied up to an energy of $E/A \sim 5$ MeV by Coimbra *et al.* [14]. In this energy region the fusion process is dominant for the ^{10,11}B + ^{11}B reactions, while the ^{10}B + ^{10}B system shows a strong limitation of the fusion cross-section even at low energies.

The ^{7}Li + ^{11}B and ^{9}Be + ^{9}Be reactions have also been studied by Mukherjee *et al.* [15] at energies up to two times the Coulomb barrier. In this work no hindrance of the fusion cross-section has been reported at energies below the Coulomb barrier, while at higher energies the fusion cross-section contributes 66% and 81%, respectively to the total reaction cross-section. In view of these facts, it is obvious that further investigation is needed in order to shed more light on the complexity of these observations. In the present work the ^{7}Li + ^{11}B system has been studied by γ-ray spectroscopy in the centre-of-mass energy region between 3.1 and 11.5 MeV. These data cover an energy range up to about 5 times the Coulomb barrier and provide useful information with regard to the behaviour of the fusion cross-section in the high-energy extreme.

[a] e-mail: vlastou@central.ntua.gr

2 Experimental procedure

The measurements were performed using the ^{7}Li beam supplied by the T11/25 Tandem Van de Graaff accelerator of the Nuclear Research Centre "Demokritos", at energies between 5.5 and 19 MeV. The target was composed of 323 μg/cm^2 of ^{11}B enriched boron, evaporated onto 100 mg/cm^2 of Ta backing. The backing ensured complete stopping of the beam in the target and was used both to monitor the beam current and to reduce the large γ-ray Doppler broadening. The target was placed in a 10 cm diameter cylindrical scattering chamber, equipped with a cold trap in order to avoid carbon build up on the target.

The beam entered the chamber through a 30 cm long tube, insulated from the rest of the beam line. This geometry helped the measurement of the beam current by collecting the charge from the whole arrangement (target, chamber and tube). For an accurate measurement of the integrated beam charge the experimental Coulomb excitation cross-sections for the 301 keV Ta γ-ray was compared with the calculated values according to the thick-target semi-classical theory of Alder *et al.* [16]. The γ-ray branching ratios of the 301 keV state to the ground state in Ta as well as the B(E2) strength and internal conversion coefficient values used in the calculations were taken from the literature [16,17].

Singles γ-ray spectra were obtained with a 95 cm^3 Ge(Li) detector at an angle of 125° and a high-purity intrinsic Ge detector at 55° with respect to the beam direction. One detector was used to accumulate detailed low energy γ-ray spectra and the other for the accumulation of all γ-rays up to 7 MeV. Since the second-order Legendre polynomial P_2 almost vanishes at 55° and 125° these spectra were taken to represent angle-integrated yields. In addition, the considerable Doppler broadening and shift at these angles allowed simple identification of γ-rays in conjunction with some low and high energy spectra taken at 90°. Both detectors were placed at a distance of 12 cm from the target and were shielded with lead to avoid beam tube background and to suppress low energy γ-rays. The relative efficiency curves of the two detectors were determined from the ^{56}Co and ^{152}Eu γ-ray spectra under the conditions of the experiment; absolute efficiencies were measured by using a standard calibrated ^{60}Co source.

Singles γ-ray spectra were taken in the range of 5.5–19.0 MeV incident ^{7}Li energy in 0.5 MeV steps. Measurements at 15.5 MeV beam energy were repeated every six hours during the experiment to check for carbon build-up. The intensity of characteristic γ-rays coming from reactions with carbon in these monitor spectra was then compared to the 136 and 301 keV peaks from the Ta backing of the target. However, at the end of the overall 100 h run time no carbon build-up on the target was observed.

Useful information concerning some reaction channels, has been extracted by using the ^{9}Be + ^{9}Be reaction, which has also been studied at the Tandem Accelerator Laboratory of the NRCPS "Demokritos" under the same experimental conditions. The two reactions ^{7}Li + ^{11}B and ^{9}Be + ^{9}Be form the same compound nucleus ^{18}O at similar excitation energies and angular momenta. Thus, they should give almost similar contributions to the various emission channels from the statistical evaporation of the compound nucleus. The study of the ^{9}Be + ^{9}Be reaction provides a means for the identification of contributions from non-compound processes.

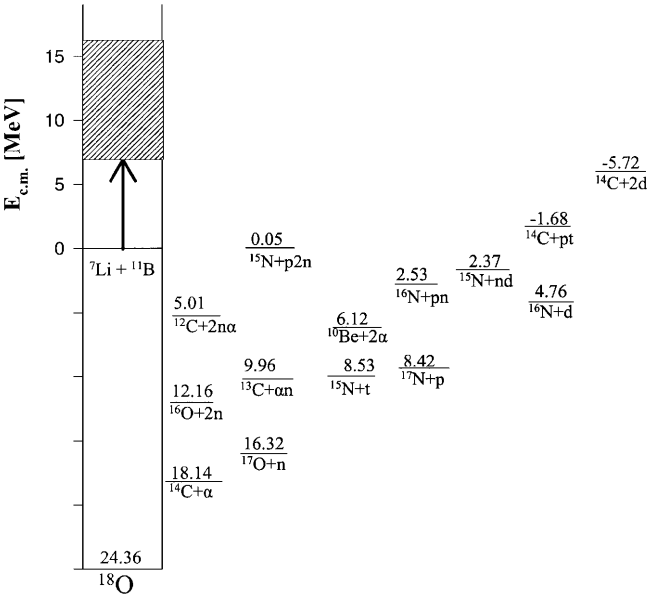

Fig. 1. Energy diagram for exit channels of the ^{7}Li + ^{11}B reaction. The cross-hatched area indicates the excitation energy in the compound nucleus ^{18}O explored in the present study.

3 Reduction of experimental data

The exit channels of the ^{7}Li + ^{11}B reaction, arranged according to binding energy, are displayed in fig. 1. A typical γ-ray spectrum obtained from this reaction at 16 MeV ^{7}Li laboratory energy and at an angle θ_γ = 125° with respect to the beam direction is presented in fig. 2. The residual nuclei produced from the evaporation of the compound nucleus by light particle emission were identified by means of their characteristic γ-rays which are summarised in table 1.

The presence of contaminants in the target, which may lead to the same residual nuclei as the ones under study, was also investigated. Contributions from the two main sources of contamination, ^{16}O and ^{12}C, were estimated as follows:

i) Oxygen-16 contamination was estimated by using the 351 keV γ-ray of ^{21}Ne produced through the ^{16}O(^{7}Li, pn) reaction. At 9.3 MeV the production cross-section of the 351 keV γ-ray has been measured by Scholz *et al.* [8] as 250 mb. Employment of this result gave for the present experiment an ^{16}O target surface density of 2.5 μg/cm^2. Oxygen-16 can contaminate mainly ^{17}O and ^{15}N exit channels through the reactions ^{16}O(^{7}Li, ^{6}Li) and ^{16}O(^{7}Li, 2α) respectively. However, from the work of Mateja *et al.* [11], it may be shown that for this surface density such contributions are negligible.

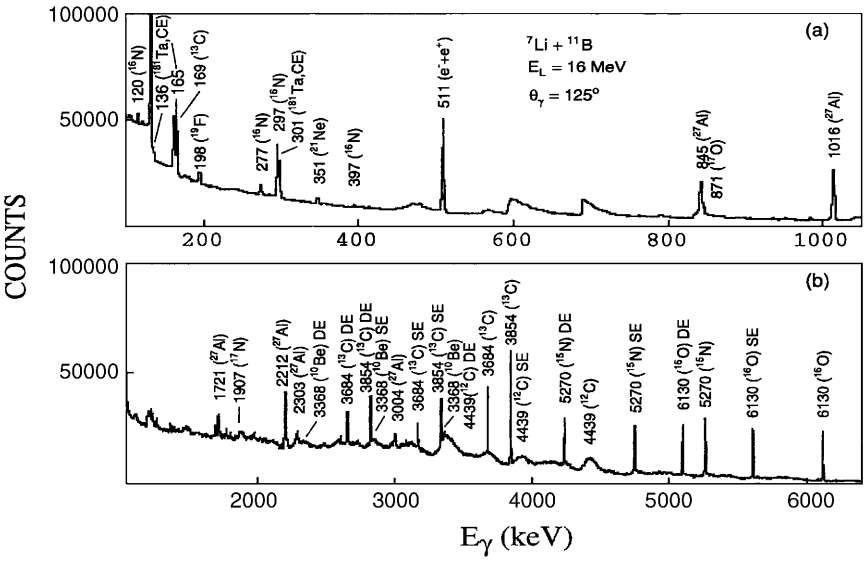

Fig. 2. Gamma-ray spectra for the ^{7}Li + ^{11}B reaction at 16 MeV ^{7}Li bombarding energy and angle of observation 125°. The energy and origin of individual photopeaks are indicated in the figure.

Table 1. Prominent γ-rays observed in the reaction ^{7}Li + ^{11} B.

Exit channel		Transitions	
Residual nucleus	Light particles	E_γ (keV)	$J_i^\Pi \rightarrow J_f^\Pi$
^{17}O	n	871	$\frac{1}{2}^+ \rightarrow \frac{5}{2}^+$
^{17}N	p	1907	$\frac{5}{2}^- \rightarrow \frac{1}{2}^-$
^{16}O	nn	6130	$3^- \rightarrow 0^+$
^{16}N	np	120	$0^- \rightarrow 2^-$
		297	$3^- \rightarrow 2^-$
		397	$1^- \rightarrow 2^-$
		277	$1^- \rightarrow 0^-$
^{15}N	t	5270	$\frac{5}{2}^+ \rightarrow \frac{1}{2}^-$
^{14}C	α	6094	$1^- \rightarrow 0^+$
		6728	$3^- \rightarrow 0^+$
^{13}C	αn	3088	$\frac{1}{2}^+ \rightarrow \frac{1}{2}^-$
		3684	$\frac{3}{2}^- \rightarrow \frac{1}{2}^-$
		3854	$\frac{5}{2}^+ \rightarrow \frac{1}{2}^-$
		169	$\frac{5}{2}^+ \rightarrow \frac{5}{2}^-$
^{12}C	αnn	4439	$2^+ \rightarrow 0^+$
^{10}Be	$\alpha\alpha$	3368	$2^+ \rightarrow 0^+$

ii) Contamination by ^{12}C was estimated from the 939 keV γ-ray of ^{18}F produced *via* the ^{12}C(^{7}Li, n) reaction. The production cross-sections for this reaction has been measured by Dennis *et al.* [12] at 10 MeV. Fluorine-18 can also be produced from ^{16}O contamination, a reaction, which has also been studied in ref. [8]. Combining these data, it was found that the surface density of ^{12}C contaminant was around 2.5 μg/cm^2. This isotope contaminates mainly ^{17}O through the reaction ^{12}C(^{7}Li, pn). We found that at 10 MeV the 871 keV peak is contaminated by about 27% from ^{12}C.

The cross-section $\sigma_{\rm res}(k)$ corresponding to the formation of a residual nucleus k can be extracted from the cross-section $\sigma_\gamma(k,i)$ of a γ-ray i emitted by this nucleus through the expression

$$\sigma_{\rm res}(k) = \frac{\sigma_\gamma(k;i)}{F_{ki}} \qquad (1)$$

in which F_{ki} is the summing and branching factor extracted from the statistical model [18,19]. The evaluation of the F factors (F_{ki}) depends on the cross-section for the excitation of each state on the residual nucleus and on the γ-ray branching ratios of these states. The γ-ray branching ratio values were taken from the literature [20] and the cross-section values from a statistical model calculation, performed using a modified version of the code STAPRE [21].

The theoretical calculations of $\sigma_\gamma(k,i)$ were carried out using values of the optical model potential parameters proposed in the literature for neutrons [22], protons [23], deuterons [24] and alphas [25] to extract the exit channel transmission coefficients. The entrance channel transmission coefficients were calculated with the Hill-Wheeler expression [26]. Numerical values of $V_{\rm B}$, $R_{\rm B}$ and $\hbar\omega$ were chosen, so that they reproduced the low-energy fusion cross-section data of the ^{7}Li + ^{11}B reaction of ref. [15]. Discrete energy levels and branching ratios for the residual nuclei, were taken from ref. [20]. The level density for all nuclei in the continuum was calculated with the Back-Shifted Fermi Gas Model [27] using the parameters of refs. [10,28]. For nuclei for which level density parameters were not available in the literature, the empirical equation for the single particle level density $a = A/10$ was used.

It should be mentioned here, that from a previous investigation of ^{13}C + ^{16}O system [19], the influence of all the parameters entering the statistical model calculations on the F factors has been extensively examined and was

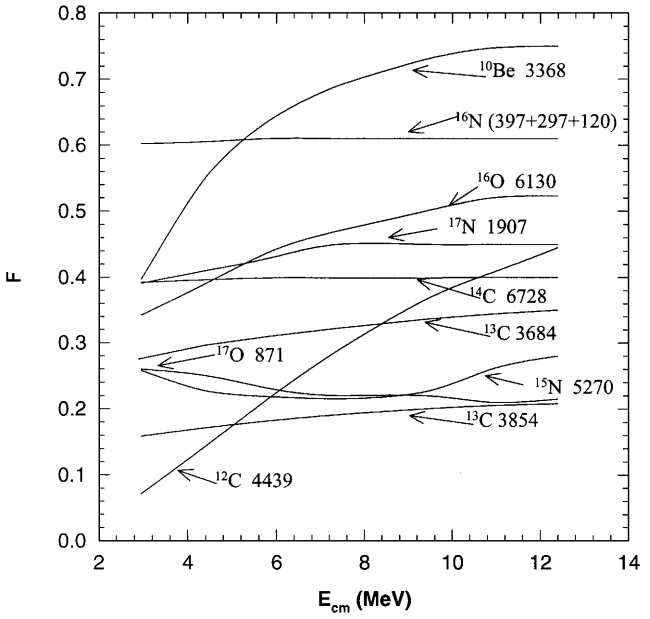

Fig. 3. Calculated F-factors for the γ-rays employed in the reduction of the data.

found to be negligible for most of the parameters. However, in order to extract reliable F factors, the influence of the entrance channel transmission coefficients to the derivation of F was further investigated by varying, the fusion barrier height $V_{\rm B}$, the radius $R_{\rm B}$ and $\hbar\omega$, within the range of their uncertainties. It was determined that such variations produced a negligible change of the values of the F factor (2%). An investigation was also undertaken with regard to the influence of level density parameters on the estimation of F factors by using two alternate sets of parameters ($a = A/10$ and $a = A/7.5$). Differences in the values of F factors calculated in this manner ranged between 5% and 12% for all exit channels, except for ^{14}C+α/tp. In this channel the calculated F factors, obtained through the two alternate sets of values for the parameter α, differ by 40% in the high-energy region and 10% in the low-energy region covered in this experiment. The uncertainties of the F factors estimated through the previous investigation were included in the value of the corresponding cross-sections calculated through eq. (1). The resulting errors varied between 5% and 15% except for the ^{14}C+α/tp. The F factors used in this work are plotted in fig. 3 and are seen to be in a very good agreement with those of the work of Mukherjee *et al.* [15].

4 Experimental results

Gamma-ray cross-sections are presented as a function of centre-of-mass energy in fig. 4, while the cross-sections for the individual exit channels are shown in fig. 5. The cross-sections of both γ-rays and reaction channels are in good agreement with those of ref. [15] in the overlapping energy region. The results are discussed in some detail below.

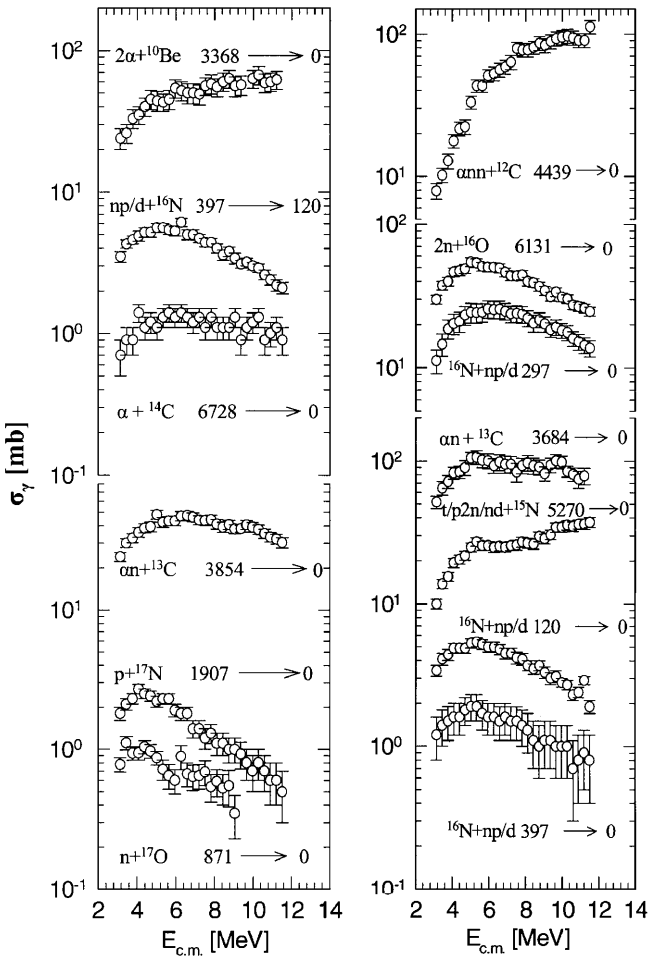

Fig. 4. Gamma-ray excitation functions for various exit channels of the ^{7}Li + ^{11}B reaction.

4.1 One-particle evaporation channels

The one-particle emission channels p + ^{17}N, n + ^{17}O and α+^{14}C contribute up to 1% each to the total fusion cross-section mainly due to their high Q-values. The d + ^{16}N and t + ^{15}N channels are much stronger (about 10% of the fusion cross-section) and are expected to start merging with the multi-particle components near the middle of the energy range covered in this experiment. These channels are discussed separately in the following sub-section.

p + ^{17}N. This channel has been derived from the 1907 keV (1907 $\rightarrow$ 0) γ-ray, which, as shown in fig. 4, carries a maximum cross-section value of 3 mb. Due to its moderate F factor ($\sim$ 40%) the deduced channel cross-section amounts to a maximum cross-section value of 7 mb (see fig. 5).

^{17}O + n. The 871 keV γ-ray of ^{17}O observed in the γ-ray spectra yields the excitation function contained in fig. 4. However, this peak is contaminated by the presence of ^{12}C on the surface of the target. Since the effect of this channel on the fusion cross-section is negligible due to its low cross-section and its moderate F factor it was decided to exclude the n + ^{17}O channel from the estimation of the total fusion cross-section.

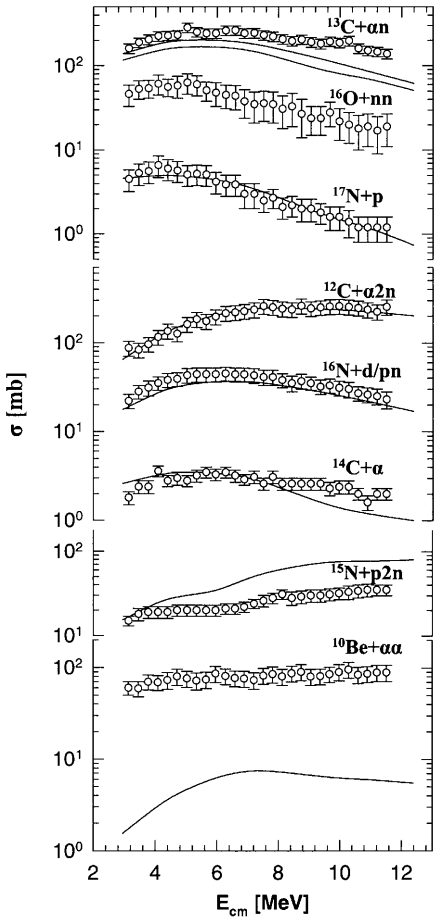

Fig. 5. Measured cross-section for population of one- two- and three-particle evaporation channels in the reaction $^{7}Li + {}^{11}B$. The full lines are the corresponding theoretical predictions from statistical model calculations using code STAPRE.

$^{14}C + \alpha$. The excitation function of this channel was estimated from the 6728 → 0 keV transition of ^{14}C, observed in the high-energy region of the spectra, not shown in fig. 2. The cross-section values of the 6728 keV γ-ray and the reaction channel are of the order of 1 mb and 3 mb, and are shown in figs. 4 and 5, respectively.

4.2 Two-particle evaporation channels

The two-particle evaporation channels contribute to the total fusion cross-section about 55% at low energies and 40% at the high-energy region covered in this experiment. The strongest channels are ^{13}C+αn and ^{10}Be+$\alpha\alpha$, and contribute approximately 45% to the total fusion cross-section. These channels are discussed separately below.

^{16}N + pn/d. Four transitions 397, 297, 277 and 120 keV were observed in this channel. The cross-section of these transitions are shown in fig. 4. The channel cross-section was deduced from the sum of the 397, 297 and 120 keV γ-rays, de-exciting the nucleus to its ground state. The F factor for the sum of the three transitions is contained in fig. 3.

$^{16}O + nn$. The cross-section for this channel was deduced through the measurement of the 6131 keV γ-ray transition, de-exciting the corresponding 3^- state with a half-life of 27 ps to the ground state of ^{16}O. The sharp 6131 keV peak in the spectra contains 66% of the ^{16}N cross-section and results from the β-decay of this nucleus to the 6131 keV level of ^{16}O. After correction for this contribution, the 6131 keV cross-section corresponding to ^{16}O population was extracted and is presented in fig. 4, while the cross-section for the direct ^{16}O channel is shown in fig. 5. The experimental results seem to agree with the data of Mukherjee *et al.* [15] within experimental errors and the uncertainties in the calculation of the F factor.

^{13}C+αn. Three transitions were seen in this strongly populated channel. Two of them, the 3854 and 169 keV de-exciting the 3.85 MeV level of ^{13}C, are sharp peaks due to the long lifetime of this level and are clearly seen in the spectra (see fig. 2). The third one, the 3684 keV γ-ray, consists of two components: a broad peak due to the short lifetime of the corresponding initial level and a sharp peak, sitting on top of the broad distribution, resulting from the de-excitation of the long-lived 3854 keV energy level through the 169 keV transition. The whole structure sits on the slope of a somehow uncertain background in this region. The ratio R of the calculated cross-section for ^{13}C production when either the 3854 keV yield or the 3684 keV yield are used, is presented in fig. 6. The deviation from the expected value of unity varies from about 10% to 20% with an associated error of about 10% due to both the experimental error and the uncertainty in the calculation of the corresponding F factors shown in fig. 3. In spite of the agreement of the two values within experimental errors, the value adopted for the formation of the ^{13}C was deduced solely from the 3854 keV transition, which was more clearly extracted from the spectra.

^{10}Be+$\alpha\alpha$. The cross-section for this channel was measured solely from the 3368 keV transition de-exciting the first excited state to the g.s. in ^{10}Be. The corresponding peak in the spectra (see fig. 2) is broadened due to the short lifetime of the initial level, but it could be easily handled during the analysis. The sharp peak sitting on top, arises from the single escape of the 3854 keV γ-ray of ^{13}C and had to be subtracted from the total yield of the broad peak. The cross-section values of the 3368 keV transition and the reaction channel are of the order of up to 70 mb and 100 mb, and are shown in figs. 4 and 5, respectively.

4.3 Three-particle evaporation channels

The three-particle evaporation channels ^{12}C+αnn and ^{15}N+t/p2n play an important role in the derivation of the total fusion cross-section. Their contribution varies from $\sim 20\%$ at low energies to $\sim 50\%$ at higher energies.

^{12}C+αnn. The cross-section for populating this channel was estimated from the 4439 keV γ-ray transition. This peak, although exhibiting considerable Doppler broadening and shifting, due to the short lifetime of the corresponding initial state, was well separated and presented no

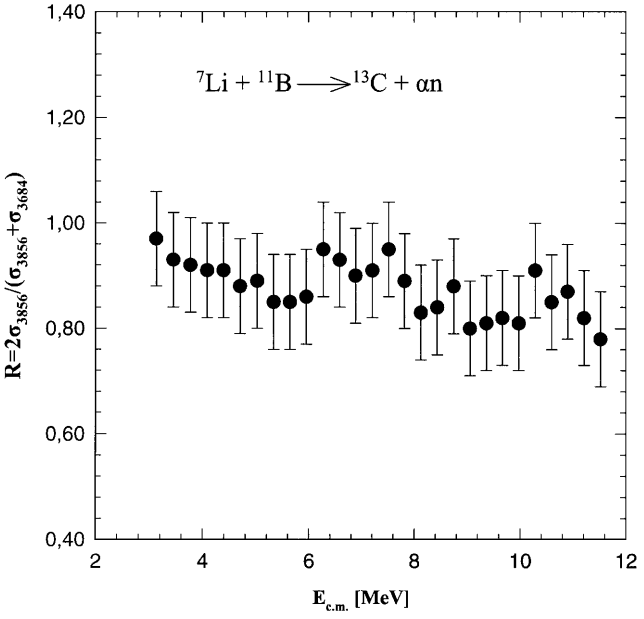

Fig. 6. The ratio of fusion cross-section estimates obtained from two alternate γ-rays for the population of ^{13}C in the reaction $^{7}\mathrm{Li} + {}^{11}\mathrm{B}$.

problems in the analysis. The channel is strong and contributes about 20% to the total fusion cross-section at low energies, while at higher energies it becomes even more important, contributing about 50% to the fusion cross-section. The cross-section values of the 4439 keV γ-ray and the derived channel cross-section are presented in figs. 4 and 5, respectively.

^{15}N+t/p2n. The population of this channel was observed through the 5270 keV transition. The peak of this γ-ray, as seen in the spectrum of fig. 2, is sharp due to the long life time of the initial state (2.6 ps), strong and well separated from neighbouring γ-rays. The cross-section of this transition is presented in fig. 4 and varies from 10 to 40 mb with increasing energy. These values are much higher than those of the corresponding one-particle channel transitions which do not carry more than 1 to 2 mb in the energy range covered here. This difference in the magnitude of the cross-section could be due to contamination from the $^{7}\mathrm{Li} + {}^{16}\mathrm{O} \rightarrow 2\alpha + {}^{15}\mathrm{N}$ reaction. As explained in Sect. 3, this contamination was estimated to be less than 1% and in any event is not consistent with the increase of the cross-section with energy. However, the latter could be attributed to multi-particle (p2n and dn) emission from the compound nucleus which is favoured at high energies. This interpretation is also corroborated by the statistical model calculations, which reveal the same qualitative behaviour with the experimental data. In addition, the F factor for the production of the 5270 keV transition, shown in fig. 3, exhibits an unusual increase in the high-energy region, caused by the appearance, as energy increases, first of the dn and then the p2n channel. The production of ^{15}N in the exit channel could also result from the α-transfer direct reaction. The 5270 keV γ-ray from the de-excitation of ^{15}N presented in fig. 4 contains both compound and non-compound processes.

In order to distinguish the compound nucleus contribution, the $^{9}\mathrm{Be} + {}^{9}\mathrm{Be} \rightarrow {}^{15}\mathrm{N}$+nnp/dn/t reaction, which is assumed to proceed through compound nucleus formation, has been employed. To this end, the experimental data of the $^{9}\mathrm{Be} + {}^{9}\mathrm{Be}$ reaction were used, with the energy shifted by 0.88 MeV (the Q-value difference of the two reactions), to produce the same excitation energy of the compound nucleus ^{18}O. The excitation function of the ^{15}N channel, extracted in this manner, is shown in fig. 5.

The total fusion cross-section presented in fig. 7, was obtained by summing the partial cross-sections for all exit channels mentioned above. The fusion cross-section measured with this γ-ray technique involves intrinsic potential difficulties. It excludes the contribution of the de-excitation of the compound nucleus by particle emission to the ground state of the evaporation residues. In the present work, this contribution has been taken into account since it is included in the theoretical estimation of the F-factors. An additional problem arises from the difficulty to distinguish between different reaction mechanisms which, contribute to some exit channels. In the case of light loosely bound systems this problem becomes even more pronounced. In the case of $^{7}\mathrm{Li} + {}^{11}\mathrm{B}$ reaction an obvious example is the ^{15}N+t/dn/p2n channel. Although, it has been taken care to correct for non compound components in ^{15}N, still the fusion cross-section extracted by this method should be regarded as an upper limit.

5 Discussion

5.1 Statistical model calculation

Statistical compound nucleus calculations were carried out in the framework of the Hauser-Feshbach theory [29], using a modified version of code STAPRE [21] in order to estimate the role of the statistical compound nucleus process in the production of residual nuclei. The values of the parameters employed in the calculations are presented in Sect. 3.

The statistical model calculations are shown in fig. 5 together with the experimental data for the various exit channels of the $^{7}\mathrm{Li} + {}^{11}\mathrm{B}$ reaction. The general trend of the excitation functions is seen to be reproduced by the calculations. For the p, αn, α2n, d/pn and α channels the calculated cross-section values are in good agreement with experimental data. However, for the p2n and nn channels the calculations are seen to overestimate the data by a factor of 2, while for the 2α channel the calculations underestimate the data by about an order of magnitude.

It is interesting to note that the same behaviour has also been observed in the calculations concerning different systems, such as $^{7}\mathrm{Li} + {}^{13}\mathrm{C}$ [10], $^{16}\mathrm{O} + {}^{13}\mathrm{C}$ [19] and $^{13}\mathrm{C} + {}^{13}\mathrm{C}$ [30]. In these systems statistical model calculations are also seen to overestimate the experimental cross-section for neutron evaporation at the expense of flux for alpha emission. In order to account for these discrepancies, several investigations have been tried using different

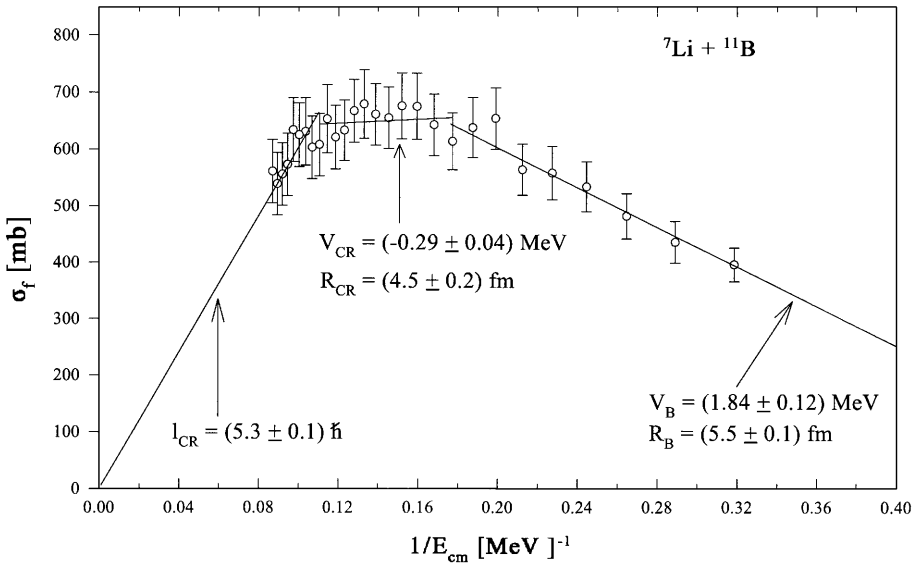

Fig. 7. The total measured fusion cross-section of the $^{7}\mathrm{Li} + {}^{11}\mathrm{B}$ reaction plotted as a function of $1/E_{\mathrm{cm}}$.

input values in the statistical model code within the limits of acceptable values. However, no progress has been achieved in this direction.

5.2 Systematics of the fusion cross-section

In general, the behaviour of the experimental fusion cross-section as a function of the inverse energy in the centre-of-mass system, for most combinations of heavy ions in the entrance channel, affords a clear division into three energy regions. The low-energy region (region I) where the bombarding energy is sufficient to overcome the Coulomb barrier and the fusion process becomes important and in fact dominates all other processes. In this region the fusion cross-section σ_{f} is nearly equal to the total reaction cross-section and is frequently described by the simple classical expression

$$\sigma_{\mathrm{f}} = \pi R_{\mathrm{B}}^2 \left(1 - \frac{V_{\mathrm{B}}}{E_{\mathrm{CM}}}\right) \tag{2}$$

in which E_{CM} is the entrance channel energy in the centre-of-mass system, R_{B} is the interaction barrier radius and V_{B} the fusion barrier height. In the intermediate energy region (region II) the fusion cross-section starts to deviate markedly from the reaction cross-section reaching a saturation value. It can be represented by the expression

$$\sigma_{\mathrm{f}} = \pi R_{\mathrm{CR}}^2 \left(1 - \frac{V_{\mathrm{CR}}}{E_{\mathrm{CM}}}\right) \tag{3}$$

in which R_{CR} is the critical radius, given in terms of the entrance channel mass numbers A_1 and A_2 as $R_{\mathrm{CR}} = r_{\mathrm{CR}}(A_1^{1/3} + A_2^{1/3})$ and V_{CR} the critical potential. Finally, in the high-energy region (region III) the fusion cross-section decreases linearly with the inverse of the incident energy. This behaviour can be attributed to the saturation of angular momentum with increasing energy and may be described by the expression (see ref. [31])

$$\sigma_{\mathrm{f}} = \frac{\pi\hbar^2 (l_{\mathrm{CR}} + 1)^2}{2\mu E_{\mathrm{F}}} \left(\frac{E_{\mathrm{F}}}{E} - 1\right), \tag{4}$$

in which l_{CR} is the limiting angular momentum, μ the reduced mass and E_{F} is the limiting energy for fusion. The fusion cross-section of the $^{7}\mathrm{Li} + {}^{11}\mathrm{B}$ reaction, shown in fig. 7, is characterised by these three regions, which can qualitatively be represented by three straight lines:

i) The solid line in region I, shown in fig. 7, represents a fit of the experimental data by eq. (2), which results for the parameter values $R_{\mathrm{B}} = (5.5 \pm 0.1)$ fm and $V_{\mathrm{B}} = (1.84 \pm 0.12)$ MeV.

ii) In region II the solid line is calculated by fitting the experimental data through eq. (3). The values of the parameters obtained from the best fit are $R_{\mathrm{CR}} = (4.5 \pm 0.2)$ fm (or $r_{\mathrm{CR}} = (1.08 \pm 0.05)$ fm) and $V_{\mathrm{CR}} = (-0.29 \pm 0.04)$ MeV.

ii) The linear expression of eq. (4) was used to fit the experimental data in energy region III. Due to the paucity of experimental data in the region of very high energy, a line intersecting the origin in fig. 7 has been chosen to fit the data. This line gives the expected trend of σ_{f} *versus* $1/E_{\mathrm{CM}}$ for a limiting angular momentum of $l_{\mathrm{CR}} = (5.3 \pm 0.1)\hbar$.

An attempt has also been made to reproduce the fusion cross-section in terms of the Glas and Mosel model [4] by fitting the data of the first two regions with the Glas-Mosel formula. The solid line shown in fig. 8 represents the result of the fitting process which yielded the values of the parameters

$$V_{\mathrm{B}} = (2.0 \pm 0.1)\,\mathrm{MeV} \quad \text{and} \quad R_{\mathrm{B}} = (5.7 \pm 0.2)\,\mathrm{fm}$$
$$(\text{or } r_{\mathrm{B}} = (1.38 \pm 0.05)\,\mathrm{fm}),$$

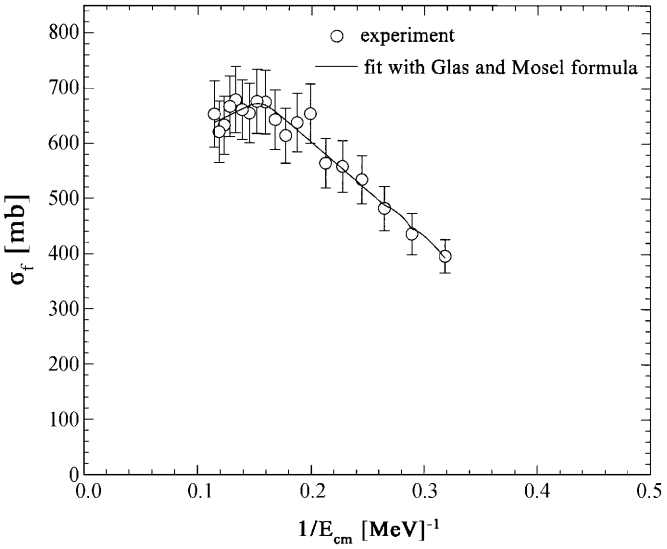

Fig. 8. The total fusion cross-section of the reaction $^{7}\mathrm{Li} + {}^{11}\mathrm{B}$, compared to predictions of the Glas-Mosel formula.

$$V_{\mathrm{CR}} = (-2.0 \pm 1.5)\,\mathrm{MeV} \quad \text{and} \quad R_{\mathrm{CR}} = (4.1 \pm 0.4)\,\mathrm{fm}$$
$$(\text{or } r_{\mathrm{CR}} = (0.99 \pm 0.08)\,\mathrm{fm}).$$

These values coincide within experimental error with the ones extracted from eqs. (2) and (3). Thus the values for barrier parameters obtained through the two procedures were averaged to give

$$V_{\mathrm{B}} = (2.0 \pm 0.1)\,\mathrm{MeV}, \qquad R_{\mathrm{B}} = (5.7 \pm 0.2)\,\mathrm{fm},$$
$$\hbar\omega = (3.0 \pm 0.7)\,\mathrm{MeV}, \qquad V_{\mathrm{CR}} = (-1.9 \pm 1.5)\,\mathrm{MeV}$$
$$\text{and } R_{\mathrm{CR}} = (4.3 \pm 0.5)\,\mathrm{fm}.$$

These potential parameter values can be compared with values deduced for other heavier ion systems. Fante *et al.* [3] have collected a large amount of fusion data between nuclei with the value of $A_1 + A_2$ ranging from 19 to 126. The potential barrier parameters for the heavier systems follow a regular behaviour as a function of the size of the system $(A_1^{1/3} + A_2^{1/3})$. However, very light systems display a discontinuity, exhibiting an anomalous increase of V_{B} and a decrease of R_{B}, resulting in a reduction of the fusion cross-section. This behaviour has been attributed to the weakly bound nuclei involved in the collision which dissociate along the reaction process opening break-up channels among the direct channels [32,33].

In the present work, though the $^{7}\mathrm{Li} + {}^{11}\mathrm{B}$ system consists of weakly bound nuclei, the barrier height deduced from the data has a much lower value than expected. It exhibits a deviation of the order of 20% relative to the systematics of heavier systems and of 50% relative to the experimental values presented in ref. [13] in the region of lighter initial systems. On the other hand, the barrier radius deduced from this work agrees within experimental error with the systematics of light ions presented in ref. [3]. In addition the maximum values of the fusion cross-section is consistent with the results presented in ref. [13] for adjacent systems. In ref. [13] a correlation between the fusion probability (ratio between fusion and reaction cross-section) and the nucleon (cluster) separation energy of the colliding nuclei has been established. For the present data, by considering the total reaction cross-section calculated from the optical model (see section 5.3) the fusion probability in the region of the plateau (region II in fig. 7) has been estimated to be around 0.6. This value is consistent with the general trend of the dependence of the fusion probability on the effective separation energy of various systems, presented in ref. [13].

A more refined approach to interpret the fusion cross-section, is the calculation of barrier penetration parameters as a function of the angular momentum, by using an analytical formula for the nuclear potential. In this calculation we have considered a nucleus-nucleus potential, which is the sum of the Coulomb, centrifugal and nuclear proximity potential of Blocki *et al.* [34]. The sharp surface radii used in the proximity potential were modified by a parameter ΔR, which was determined by fitting the expression of the proximity model to the fusion cross-section data. The fitted value of ΔR which best reproduces the experimental data was 0.03 fm and leads to values for the potential parameters of $R_{\mathrm{B0}} = 6.5\,\mathrm{fm}$ and $V_{\mathrm{B0}} = 2.3\,\mathrm{MeV}$ for $l = 0$.

It is further possible to consider the dependence of the fusion cross-section on energy by investigating angular-momentum limitations for forming the compound nucleus. The maximum angular momentum for fusion l_{f} may be extracted from the fusion cross-section data by using the sharp cut-off approximation according to the expression

$$\sigma_{\mathrm{f}} = \pi\lambda\!\!\!^{-2} \sum_{l=0}^{l_{\mathrm{f}}} (2l+1) = \pi\lambda\!\!\!^{-2}(l_{\mathrm{f}}+1)^2. \qquad (5)$$

However, in the system considered here, the channel spin ranges from 0 to $3\hbar$, due to the intrinsic spin values $3/2^-$ of the nuclei $^{7}\mathrm{Li}$ and $^{11}\mathrm{B}$, which is comparable to the values of the angular momentum brought into the system. Thus it is more appropriate to describe the fusion process with the cut-off made on the total angular momentum J_{f} of the compound nucleus. This value has been deduced from the experimental data of the $^{7}\mathrm{Li} + {}^{11}\mathrm{B}$ reaction by using the expression

$$\sigma_{\mathrm{f}} = \sum_{J=0}^{J_{\mathrm{f}}} \pi\lambda\!\!\!^{-2} \frac{2J+1}{(2I_a+1)(2I_A+1)} \sum_{S=|I_a-I_A|}^{I_a+I_A} \sum_{l=|J-S|}^{J+S} T_l, \quad (6)$$

where S is the channel spin, as given from the coupling of the projectile and target spins I_a and I_A, l is the orbital angular momentum and l_{f} is the maximum angular momentum for fusion. The transmission coefficients T_l can be approximated by the usual step function $\theta(l_{\mathrm{f}} - l)$ [11].

The experimental total angular momentum J_{f} of the compound nucleus $^{18}\mathrm{O}$ deduced from this work is shown in fig. 9 (open circles) as a function of excitation energy of the system E^*. Additional values of J_{f}, extracted from the data of ref. [15], have also been plotted for the $^{9}\mathrm{Be} + {}^{9}\mathrm{Be}$ reaction (squares), which leads to the same

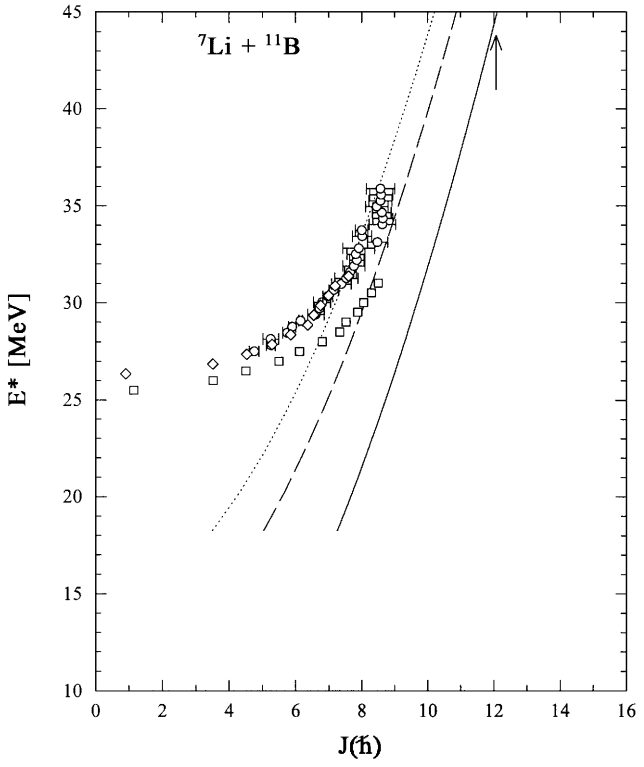

Fig. 9. Total angular momentum for fusion J_{f} as a function of excitation energy of the compound nucleus ^{18}O. The results of the present work are denoted as open circles. The diamonds and the squares are extracted from ref. [15] for $^{7}\mathrm{Li} + {}^{11}\mathrm{B}$ and $^{9}\mathrm{Be} + {}^{9}\mathrm{Be}$ systems, respectively. The solid is the yrast line, while the dashed and the dotted lines are the statistical yrast lines extracted from systematics [5] and fit to the data, respectively. The vertical arrow indicates the limiting angular momentum for fission, predicted by rotating liquid-drop model.

compound nucleus. In this case eq. (6) is modified by a factor $[l + (-l)^{l+S}]$, since the nuclei participating in the reaction are identical. In order to clarify the energy dependence of J_{f} additional experimental values have also been deduced from the low energy fusion cross-section of ref. [15] for the $^{7}\mathrm{Li} + {}^{11}\mathrm{B}$ reaction, and are presented in fig. 9 as diamonds.

The yrast line, shown in fig. 9 as a solid line, is extracted by assuming that the composite system is a rigid rotor with a reduced radius of $r_0 = 1.25\,\mathrm{fm}$. The yrast line represents an absolute limit for the formation of the compound nucleus ^{18}O with the nuclear temperature equal to zero. Vanderbosch and Lazzarini [6] have proposed that the fusion cross-section is limited by the available nuclear states of the compound nucleus. This means that the level spacing D must be less than the average width Γ for all l values leading to fusion, implying a nuclear temperature greater than zero. The level spacing $D = 1/\rho$ has been estimated by using the back-shifted Fermi-Gas model for level density ρ [27], assuming the same parameters as those used for the statistical model calculations in this work. The value of the ratio Γ/D, which fits the trajectory of the maximum total angular momentum J_{f}, is 100 and corresponds to a minimum value of nuclear temperature 2.5 MeV, above which the participating nuclei tend to fuse. These values would not justify a limitation of the fusion cross-section caused by the available states of the compound nucleus.

With regard to compound nucleus limitations, Lee *et al.* [5] have proposed the existence of a "Statistical yrast line" above which the level density becomes large enough in order for fusion to occur. In this representation the statistical yrast line is assumed to run nearly parallel to the physical yrast line and shifted by the additional energy ΔQ. Systematic study of various light-heavy ion systems [5] revealed that the parameter ΔQ does not depend on the entrance channel and is roughly constant with a value $\Delta Q = (10.0 \pm 2.5)\,\mathrm{MeV}$. The corresponding yrast line is presented in fig. 9 as dashed line. By using the expression of Lee *et al.* [5], the experimental data in the intermediate energies of the present reaction have been fitted and the optimum value of ΔQ was found to be $\Delta Q = (14 \pm 2)\,\mathrm{MeV}$ with $r_0 = 1.25\,\mathrm{fm}$, which is close to the one deduced from the systematic study. The statistical yrast line using this value of ΔQ obtained here is shown in fig. 9 as a dotted line.

Civitarese *et al.* [35] defined the intrinsic energy ΔQ needed for fusion, as a function of the atomic mass number A_{CN} of the compound system ($\Delta Q = 0.27 A_{\mathrm{CN}}$). The line resulting from this calculation has exactly the same slope as the one proposed by Lee *et al.*, but for a given angular momentum is shifted to lower energies by about 5 MeV due to the difference of the ΔQ values. This line lies much closer to the yrast line, but exhibits a large deviation from the experimental data compared to the statistical yrast line proposed by Lee *et al.* [5]. The value of ΔQ extracted from the present data tends to be higher than the values deduced from the systematics of Lee *et al.* [5] and Civitarese *et al.* [35], indicating that higher density of states is needed in order to ensure the fusion process. This shift of the "Statistical Yrast Line" towards higher temperatures could be attributed to the loosely bound nature of the participating ions.

At higher energies, it is seen that the limiting angular momentum J_{f} tends to a constant value of $8.5\hbar$. In order to interpret this saturation of J_{f}, the critical total angular momentum for fission has been estimated within the framework of the Rotating Liquid Drop Model (RLDM) (as refined by Sierk *et al.* [36] and Mustafa *et al.* [37]), to be around $12\hbar$. The experimental $J_{\mathrm{f}} = 8.5\hbar$ does not reach this value of the total angular momentum that the compound nucleus can support in terms of the RLDM. However, it should be kept in mind that in the case of light nuclei such as ^{18}O, this RLDM prediction may carry large uncertainties due to shell effects and to the assumption that these light nuclei are described as sharp surface liquid drops [38].

The total angular momentum J_{f} that the compound nucleus ^{18}O can afford, extracted from the data of $^{9}\mathrm{Be} + {}^{9}\mathrm{Be}$ system [15], is also presented in fig. 9. In the low-energy region the two curves run parallel and are shifted by about 1 MeV indicating that the lighter ^{7}Li

projectile carries less angular momentum for the same excitation energy of the compound nucleus. At higher energies it appears to be some evidence for a common limitation around $8.5\hbar$. However, more experimental data for ^{9}Be + ^{9}Be reaction are needed at higher energies to ensure this saturation and confirm a compound nucleus limitation process.

5.3 Optical model analysis

In order to estimate the contribution of the total fusion cross-section to the total reaction cross-section of the ^{7}Li + ^{11}B reaction in the energy range covered in this experiment, an optical model analysis has been performed using various sets of potential parameters taken from the literature. These calculations were carried out using code ATHREE [39], specially suited to heavy-ion reactions.

The only elastic scattering data available for ^{7}Li + ^{11}B, are those of Kohler *et al.* [40] measured at 14.7 MeV energy in the centre-of-mass system, which is about 3 MeV above the highest energy in the present work. In order to have a rough estimation of the reaction cross-section, the optical model parameters of ref. [40] have been used for the whole energy range. The results seem to approach the fusion cross-section at low energies even though the parameters correspond to higher energy data. In the high-energy region the reaction cross-section overestimates the measured fusion cross-section, reaching a deviation of the order of 50% at 12 MeV CM energy. Similar results have also been extracted by using the optical model potential deduced from the elastic scattering data of the neighbouring systems ^{6}Li + ^{12}C and ^{7}Li + ^{12}C [41] over an extended energy range, after appropriate radius modification.

In all cases mentioned above the contribution of the fusion cross-section to the total reaction cross-section decreases considerably with increasing energy. This behaviour is attributed to binary processes, which become important at high energies. These processes, apart from the direct transfer may include the formation of a dinuclear system which lives long enough to increase the probability for cluster transfers [42,43] even at sub-barrier energies. Such processes are expected to be pronounced in the case of the ^{9}Be + ^{9}Be system (which produces the same compound nucleus as ^{7}Li + ^{11}B at similar excitation energies), caused by the loosely bound ^{9}Be nuclei. Since elastic scattering cross-section data for the ^{9}Be + ^{9}Be system exist [44–46] at CM energies between 2.2 and 25 MeV, reliable optical model parameters are available in the literature from fitting these data. Thus, the parameters extracted from ref. [46] have been used to estimate the reaction cross-section of the ^{7}Li + ^{11}B reaction. The results overestimate the fusion cross-section even more than in the previously mentioned calculations. However, this difference is expected since the contribution of both direct and transfer reactions changes when the reaction is induced by ^{7}Li or by ^{9}Be nuclei.

6 Summary

The cross-section of the individual evaporation channels and the total fusion cross-section for the ^{7}Li + ^{11}B reaction have been measured through the observation of single γ-rays.

In the centre-of-mass energy range 3.1–11.5 MeV examined in this work, the experimental cross-section in the various exit channels reveal that the αn and α2n are the strongest channels and contribute up to 80% to the total fusion cross-section.

The overall trend of the excitation function of the individual channels measured here was satisfactorily accounted for by statistical model calculations. However, these calculations seem to overestimate the experimental cross-section for neutron evaporation channels at the expense of flux for alpha particle emission. The interaction barrier height $V_{\rm B}$ and radius $R_{\rm B}$ have been extracted from low-energy fusion cross-section data by using the Glas-Mosel model. The barrier height is lower with regard to systematics behaviour [3], while the barrier radius is consistent with values of neighbouring systems.

At high energies, above $4V_{\rm B}$, the fusion cross-section exhibits a substantial decrease as energy increases. The total angular momentum brought into the compound nucleus ^{18}O evinces a saturation with energy, which can be associated with the asymptotic properties of the compound nucleus. This behaviour could be attributed to the available states of the compound nucleus. However, an estimation of the level spacing and the average width for all J values leading to fusion do not justify this concept [6]. On the other hand the limiting value of the total angular momentum is deduced from the experimental data to be $8.5\hbar$, which does not reach the value of the total angular momentum $12\hbar$ that the compound nucleus can support in terms of the rotating liquid drop model. In addition, the total angular momentum extracted from the experimental data of the ^{9}Be + ^{9}Be system [15], leading to the same compound nucleus ^{18}O, exhibits similar tendency for saturation at about the same value of $8.5\hbar$. It is realised that further experimental data at higher energies are needed for this system in order to conclude whether the inhibition of the fusion cross-section is imposed by the compound nucleus.

C. Tsabaris would like to thank IKY for the continuous support and the Physics Department of NTUA for the hospitality.

References

1. D.G. Kovar, D.F. Geesaman, T.H. Braid, Y. Eisen, W. Henning, T.R. Ophel, M. Paul, K.E. Rehm, S.J. Sanders, P. Sperr, J.P. Schiffer, S.L. Tabor, S. Vigdor, B. Zeidman, F.W. Prosser Jr., Phys. Rev. C **20**, 1305 (1979).
2. J.R. Birkelund, L.E. Tubbs, J.R. Huizenga, J.N. De, D. Sperber, Phys. Rep. **56**, 107 (1979).
3. L. Fante Jr., N. Added, R.M. Anjos, N. Carlin, M.M. Coimbra, M.S.C. Figueira, R. Matheus, E.M. Szanto de Toledo, Nucl. Phys. A **552**, 82 (1993).

4. D. Glas, U. Mosel, Phys. Rev. C **10**, 2620 (1974).
5. S.M. Lee, T. Matsuse, A. Arima, Phys. Rev. Lett. **45**, 165 (1980).
6. R. Vanderbosch, A.J. Lazzarini, Phys. Rev. C **23**, 1074 (1981).
7. A.R. Omar, J.S. Eck, T.R. Ophel, J.R. Leigh, Phys. Rev. C **30**, 1516 (1984).
8. C.J.S. Scholz, L. Ricken, E. Kuhlmann, Z. Phys. A **325**, 203 (1986).
9. A. Mukherjee, U. Datta Pramanik, S. Chattopadhyay, M. Saha Sarkar, A. Goswami, P. Basu, S. Bhattacharya, M.L. Chatterjee, B. Dasmahapatra, Nucl. Phys. A **635**, 305 (1998).
10. A. Mukherjee, U. Datta Pramanik, M. Saha Sarkar, A. Goswami, P. Basu, S. Bhattacharya, S. Sen, M.L. Chatterjee, B. Dasmahapatra, Nucl. Phys. A **596**, 299 (1996).
11. J.F. Mateja, J. Garman, D.E. Fields, R.L. Kozub, A.D. Frawley, L.C. Dennis, Phys. Rev. C **30**, 134 (1984).
12. L.C. Dennis, K.M. Abdo, A.D. Frawley, K.W. Kemper, Phys. Rev. C **26**, 981 (1982).
13. J. Takahasi, M. Munhoz, E.M. Szanto, N. Carlin, N. Added, A.A.P. Suaide, M.M. de Moura, R. Liguori Neto, A. Szanto de Toledo, Phys. Rev. Lett. **78**, 30 (1996).
14. M.M. Coimpra, R.M. Anjos, N. Adder, N. Carlin Filho, L. Fante Jr., M.C.S. Figueira, G. Ramirez, E.M. Szanto, A. Szanto de Toledo, Nucl. Phys. A **535**, 161 (1991).
15. A. Mukherjee, B. Dasmahapatra, Nucl. Phys. A **614**, 238 (1997).
16. K. Alder, A. Bohr, T. Huus, B. Mottelson, A. Winther, Rev. Mod. Phys. **28**, 432 (1956).
17. P.R. Sharma, Nucl. Phys. A **154**, 312 (1970).
18. Z.E. Switkowski, R.G. Stokstad, R.M. Wieland, Nucl. Phys. A **274**, 202 (1976).
19. C.T. Papadopoulos, R. Vlastou, E.N. Gazis, P.A. Assimakopoulos, C.A. Kalfas, S. Kossionides, A.C. Xenoulis, Phys. Rev. C **34**, 196 (1986).
20. P.M. Endt, Nucl. Phys. A **521**, 1 (1990); F. Ajzenberg - Selove, Nucl. Phys. A **152**, 1 (1970); Nucl. Phys. A **268**, 1 (1976); Nucl. Phys. A **475**, 1 (1987); Nucl. Phys. A **490**, 1 (1988); Nucl. Phys. A **506**, 1 (1990); Nucl. Phys. A **523**, 1 (1991); D.R. Tilley, H.R. Weller, C.M. Cheves, Nucl. Phys. A **564**, 1 (1993).
21. M. Uhl, Acta Phys. Austriaca **31**, 245 (1970).
22. D. Wilmore, P.E. Hodgson, Nucl. Phys. **55**, 673 (1964).
23. F.G. Perey, Phys. Rev. **131**, 745 (1975).
24. C.M. Perey, F.G. Perey, Phys. Rev. **132**, 755 (1963).
25. J.R. Huizenga, G. Igo, Nucl. Phys. **29**, 462 (1962).
26. D.L. Hill, J.A. Wheeler, Phys. Rev. C **89**, 1102 (1953).
27. H.K. Vonach, I. Hille, Nucl. Phys. A **127**, 289 (1969).
28. D.W. Lang, Nucl. Phys. **26**, 434 (1961).
29. W. Hauser, H. Feshbach, Phys. Rev. **87**, 366 (1952).
30. J.L. Charvet, R. Dayras, J.M. Fieni, S. Joly, J.L. Uzureau, Nucl. Phys. A **376**, 292 (1982).
31. H. Morgenstern, W. Bohne, K. Grabisch, H. Lehr, W. Stöffler, Z. Phys. A **313**, 39 (1983).
32. M.C.S. Figueira, E.M. Szanto, A. Szanto de Toledo, M.P. Pato, M.S. Hussein, L.F. Canto, Phys. Rev. C **46**, 1139 (1992).
33. N. Soić, D. Cali, S. Cherubini, E. Costanzo, M. Lattuada, M. Millin, D. Miljanić, S. Romano, C. Spitaleri, M. Zadro, Eur. Phys. J. A **3**, 303 (1998)
34. J. Blocki, J. Randrup, W.J. Swiatecki, C.F. Tsang, Ann. Phys. **105**, 427 (1977).
35. O. Civitarese, B.V. Carlson, M. S. Hussein, A. Szanto De Toledo, Phys. Lett. **125**, 22 (1983).
36. A.J. Sierk, Phys. Rev. C **33**, 2039 (1986).
37. M.G. Mustafa, P.A. Baisden, H. Chandra, Phys. Rev. C **25**, 2524 (1985).
38. J. Blocki, K. Grotowski, R. Planeta, W.J. Swiatecki, Nucl. Phys. A **445**, 367 (1985).
39. E.H. Auerbach, Comput. Phys. Commun. **15**, 165 (1978).
40. W. Kohler, H. Schmidt-Bocking, K. Bethge, Nucl. Phys. A **262**, 888 (1976).
41. J.E. Poling, E. Norbeck, R.R. Carlson, Phys. Rev. C **13**, 648 (1976).
42. B. Dasmahapatra, B. Cujec, F. Lahlou, I.M. Szoghy, Nucl. Phys. A **509**, 393 (1990).
43. B. Dasmahapatra, B. Gujec, G. Kajrys, J.A. Cameron, Nucl. Phys. A **564**, 314 (1993).
44. F. Lahlou, B. Cujec, B. Dasmahapastra, Nucl. Phys. A **486**, 189 (1988).
45. R.C. York, R.T. Carpenter, Nucl. Phys. A **282**, 351 (1977).
46. A.R. Omar, J.S. Eck, J.R. Leigh, T.R Ophel, Phys. Rev. C **30**, 896 (1984).